

Supporting Information

Hybrid Nanoreceptors for High Sensitivity Detection of Small Molecules by NMR Chemosensing

Federico De Biasi,^[a,b] Daniele Rosa-Gastaldo,^[a] Fabrizio Mancin,^[a] and Federico Rastrelli^[a]

^[a] Department of Chemical Sciences, Università degli Studi di Padova, Via Marzolo 1, 35131 Padova (Italy)

^[b] Department of Chemistry, Università degli Studi di Firenze, Via della Lastruccia 3-13, 50019 Sesto Fiorentino (Italy)

Table of Content

1. Theoretical aspects	S1
2. Synthesis and characterization of 1 -AuNPs and 2 -AuNPs	S3
3. Size of LUDOX [®] nanoparticles	S8
4. DLS experiments	S9
5. Composition of the nanoconjugates	S11
6. Samples preparation and NMR pulse sequences	S12
7. Additional NMR experiments	S13
8. Synthesis of thiols T1 and T2	S15
9. References	S17

1. Theoretical aspects

The results reported in the main text can be explained on the basis of a rudimentary model for the interaction between an analyte (the guest, G) and a gold nanoparticle (the host, H), epitomized by the equilibrium reported in (1). Here, the affinity constant K_a is defined as the ratio between the kinetic rates of association and dissociation k_{on} and k_{off} of the complex.



In STD experiments, the monolayer's magnetization is saturated by an RF irradiation and partly transferred to the interacting species during the binding events.¹ The spin-spin interactions responsible for the NOE in the bound state are very short-ranged, so it is possible to model the magnetization transfer as an "on-off" process that is active only when the analytes are in long-lived association with the monolayer. The influence of the rotational correlation time of the AuNPs on the NOE enhancement in STD-based NMR chemosensing experiments can be unveiled assuming that both the species H and G comprise only one spin each. This hypothesis is clearly not representative of the real situation, but it allows us to derive the fundamental principles at the basis of the experimental observations. The equilibrium (1) can be hence expressed in terms of spins I and S , respectively for G and H, as:²



The suffixes “f” and “b” are used to denote the free and bound states. Under the assumptions that the host’s spin (spin S) is saturated in both states (*i.e.* the resonance frequency of S does not vary significantly between the free and bound states, hence the RF field irradiates both) and a steady-state magnetization transfer is achieved (which is typical of STD spectroscopy), two expressions for the NOE enhancement on spin I in the free and bound states can be derived.

$$\eta_{lf} = \frac{\sigma_{IS} k_{on} [H]}{k_{off} \rho_{1,lf} + k_{on} [H] \rho_{IS} + \rho_{1,lf} \rho_{IS}} \quad (3.1)$$

$$\eta_{lb} = \frac{\sigma_{IS} (k_{on} [H] + \rho_{1,lf})}{k_{off} \rho_{1,lf} + k_{on} [H] \rho_{IS} + \rho_{1,lf} \rho_{IS}} \quad (3.2)$$

$\rho_{1,lf}$ is the longitudinal relaxation rate of spin I in the free state, ρ_{IS} and σ_{IS} are the auto- and cross-relaxation rates at the basis of the NOE in the bound state and [H] is the molar concentration of the host. See reference 2 for a more detailed derivation of equations (3.1) and (3.2).

In fast chemical exchange conditions, where both k_{off} and $k_{on}[H]$ are much larger than the NMR relaxation rates present in (3.1) and (3.2) and a single averaged NMR resonance is observed for I, the total NOE enhancement is:

$$\eta_{tot} = \frac{\rho_b \sigma_{IS}}{\rho_f \rho_{1,lf} + \rho_b \rho_{IS}} = \frac{\rho_b \sigma_{IS}}{(1 - \rho_b) \rho_{1,lf} + \rho_b \rho_{IS}} \quad (4)$$

Here, the populations of the free and bound G states, ρ_f and ρ_b , have been introduced ($\rho_f + \rho_b = 1$). Equation (4) is very similar to the well-known expression for the NOE enhancement in a homonuclear two spin-1/2 system ($\eta = \sigma_{IS}/\rho_{IS}$) that nonetheless represents the maximum theoretical value of (4), valid when $\rho_f = 0$ and $\rho_b = 1$. Shifting the host-guest equilibrium towards the bound state using large quantities of AuNP increases the overall enhancement η_{tot} , but it also broadens the resonances of the interacting species, causing hence a strong decrement of the signal-to-noise ratio of the peaks of interest.³

On the other hand, the augmentation of the receptor’s rotational correlation time can improve the detection limit in saturation transfer experiments: this not only favours the spin diffusion process within the receptor itself but also minimizes the contribution of the free substrate’s relaxation in (4) which lowers the absolute value of η_{tot} . Indeed, both ρ_{IS} and σ_{IS} depend on the correlation time of the spins in the bound state, which in turn depends on the rotational correlation time of the receptor as follows:⁴

$$\frac{1}{\tau_b} = \frac{1}{\tau_C} + \frac{1}{\tau_{res}} = \frac{1}{\tau_C} + k_{off} \quad (5)$$

where τ_b is the spin correlation time in the bound state, τ_C is the overall rotational correlation time of the receptor and $\tau_{res} = k_{off}^{-1}$ is the mean residence time of the guest in the host’s binding site (no internal motions are considered). At 300 K in water, τ_C is of the order of 10 ns for 2 nm AuNPs while it is of the order of 10 μ s for the nanoconjugates, being the size of the latter about 10 times larger than that of the AuNPs. Assuming a Lorentzian spectral density function characterized by a correlation time τ_b and

expressing ρ_{IS} and σ_{IS} as linear combinations of such spectral density at $\omega = 0$, ω_0 and $2\omega_0$ (with ω_0 being the Larmor frequency of the homonuclear spin pair),⁵ it is possible to compute the total NOE enhancement as a function of τ_C . Results are reported in Figure S1.

As the receptor's size does grow, the values of ρ_{IS} and σ_{IS} increase in magnitude. For low bound fractions, the total NOE enhancement is significant only in the presence of sufficiently large receptors. Generally speaking, low bound fractions are required in NMR ligand-receptors analysis to avoid a severe broadening of the signals of the interacting species.

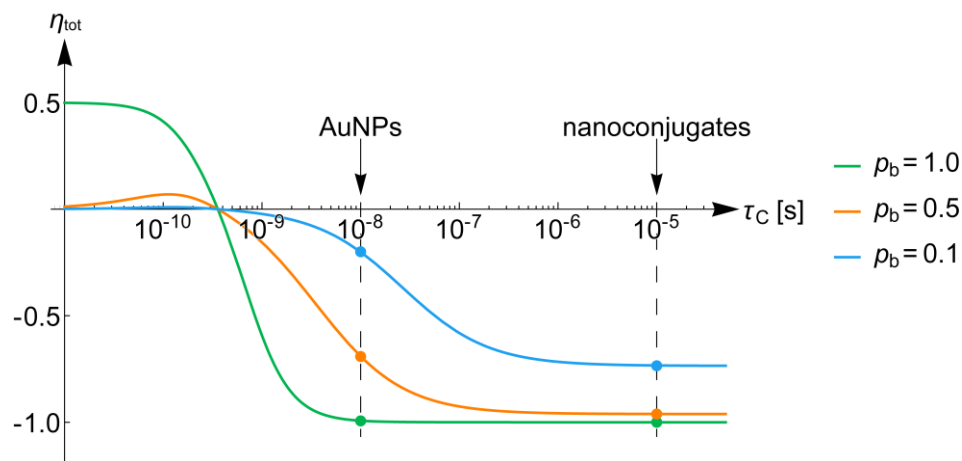


Figure S1: Total NOE enhancements as a function of the receptor's rotational correlation time for different bound fractions of the guest species. The following parameters were fixed in the numerical calculation: $\omega_0 = -2\pi 500 \times 10^6 \text{ rad s}^{-1}$, $\rho_{1,if} = 1 \text{ s}^{-1}$, $k_{off} = 10^7 \text{ s}^{-1}$. Spins in the bound state were assumed to be separated by 3 Å. In the presence of high bound fractions (green and orange curve), the total NOE enhancement is strong for both the AuNPs and the nanoconjugates, but the linewidth of the resonances of the interacting species is expected to be rather broad.³ On the contrary, in the presence of a low bound fraction (light blue curve), the total NOE enhancement is significant only for a sufficiently high receptor's rotational correlation time.

It is worth noting that fast chemical exchange conditions between the analytes and the coating monolayer are still valid even in the presence of the nanoconjugates, as only one set of resonances for the interacting species is observed experimentally. In addition, the nanoconjugates could be characterized by regions in which the analytes can be trapped and become invisible to the NMR detection. Nonetheless, a careful comparison between the $^1\text{H-NMR}$ spectra of the investigated mixtures recorded in the absence and in the presence of the AuNPs@SiO₂NPs nanoconjugates did not report any significant variation in the resonance intensities for the interacting species, indicating that such phenomena are absent or completely negligible in the investigated cases.

2. Synthesis and characterization of 1-AuNPs and 2-AuNPs

1-AuNPs and 2-AuNPs were prepared following a previously reported procedure.⁶ A solution of HAuCl₄·3H₂O (50 mg, 0.127 mmol, 1 equiv) in water (1 mL) is extracted with a solution of tetraoctylammonium bromide (0.175 g, 0.318 mmol, 2.5 equiv) in degassed toluene (125 mL). Dioctylamine (0.613 g, 2.539 mmol, 20 equiv, suitable for 2 nm AuNPs) is then added. The mixture is stirred under N₂ for 1,5 hours. Then the solution is cooled at 0°C (ice-water bath) and a NaBH₄ solution (48.0 mg, 1.269 mmol, 10 equiv) in water (1 mL) is rapidly added. The colour of the solution turns rapidly to black and after 1.5 hours of ageing at 0°C, the aqueous layer is removed. To the obtained

nanoparticle solution, the thiol is added (0.254 mmol, 2 equiv) dissolved in 3 mL of MeOH. The reaction mixture is stirred overnight from 0°C to room temperature.

The AuNPs were purified through precipitation in different solvent mixtures and through gel permeation chromatography with Sephadex G-25 using water as eluent.

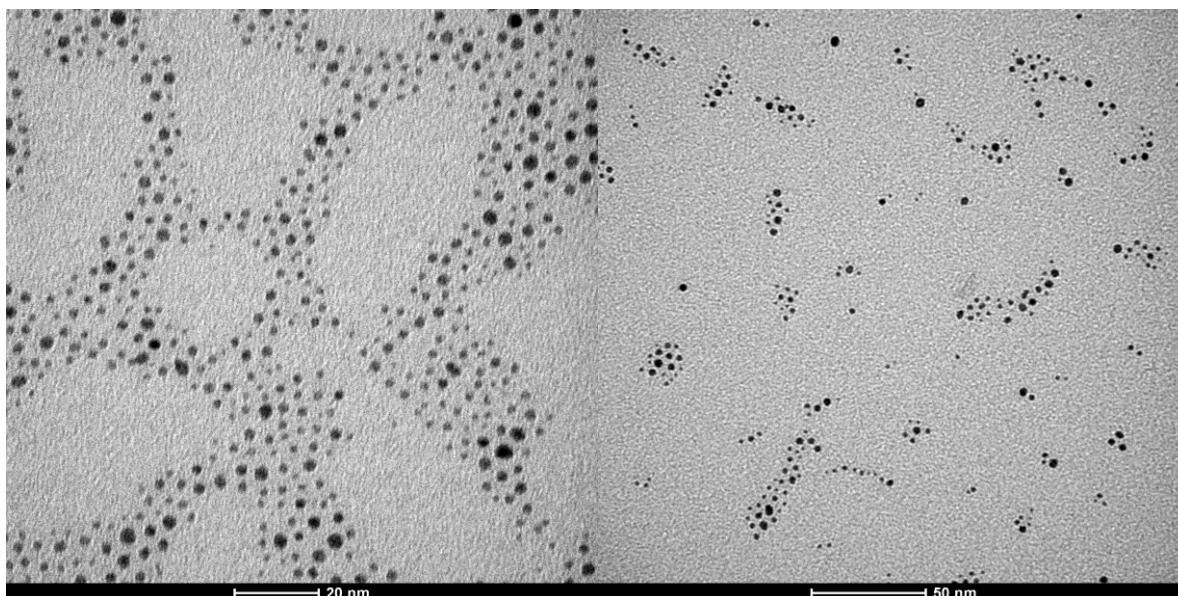


Figure S2: TEM images of a solution 1-AuNPs (1 mg/mL).

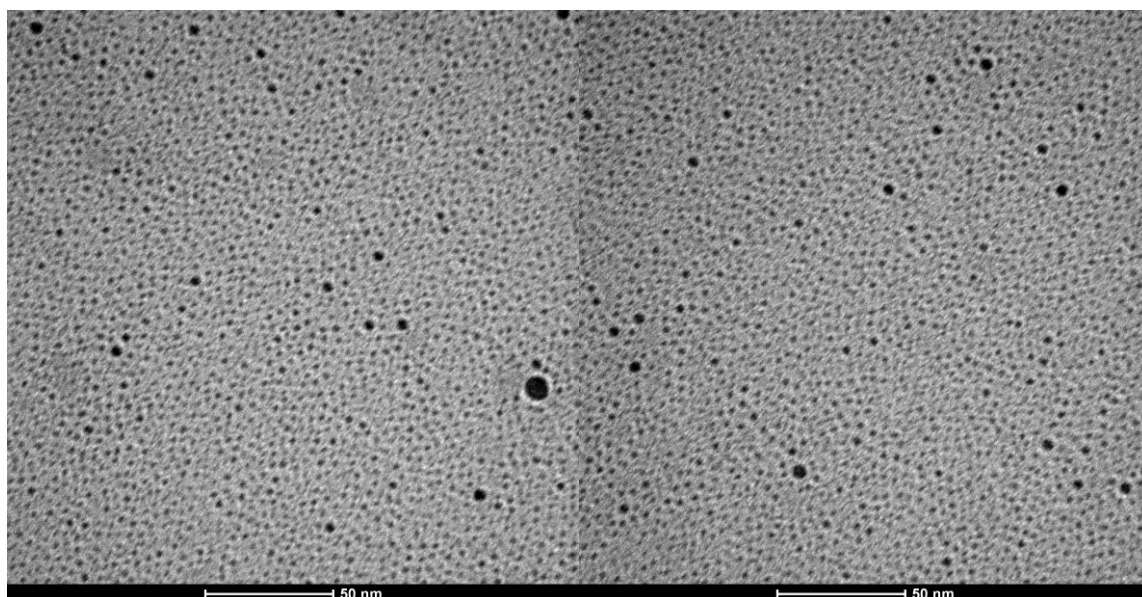


Figure S3: TEM images of a solution 2-AuNPs (1 mg/mL).

TEM images were recorded on a Jeol 300 PX electron microscope. One drop of sample was placed on the sample grid and the solvent was removed with filter paper. TEM images were analysed with ImageJ.

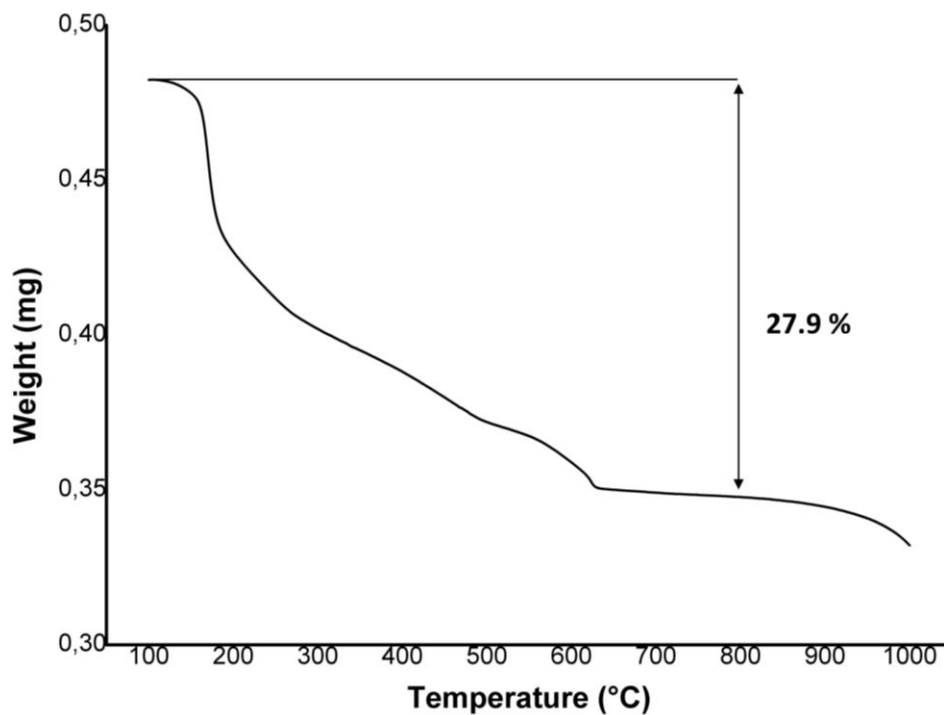


Figure S4: TGA analysis of 1-AuNPs (0.48 mg). Weight loss 27.9% (ramp 10 °C/min, 100-1000 °C, air atmosphere).

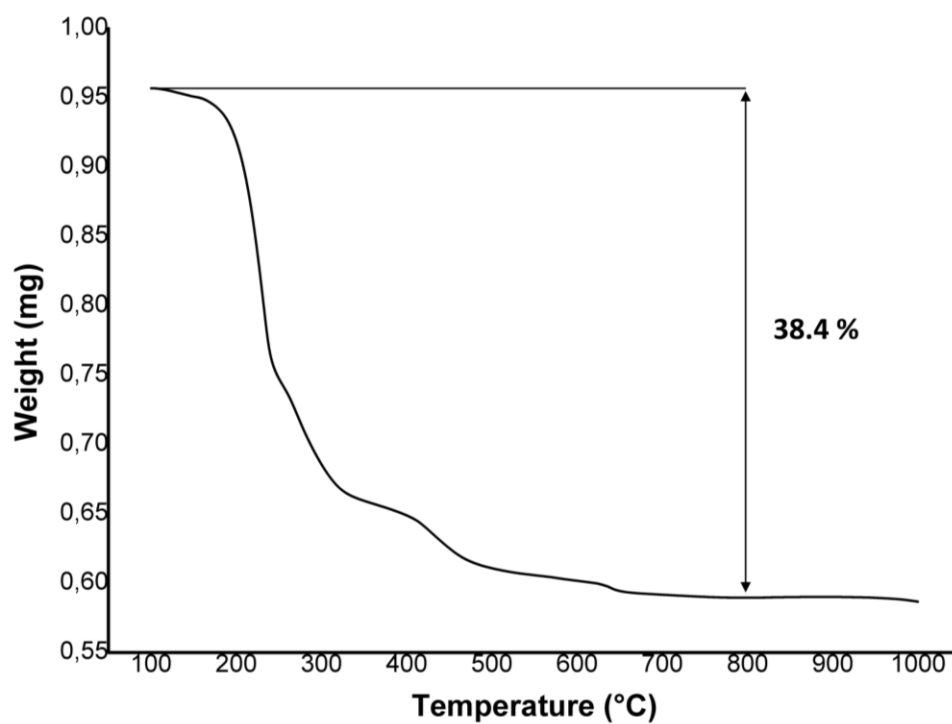


Figure S5: TGA analysis of 2-AuNPs (0.96 mg). Weight loss 38.4% (ramp 10 °C/min, 100-1000 °C, air atmosphere).

TGA were run using a Q5000 IR model TA instrument under a continuous air flow.

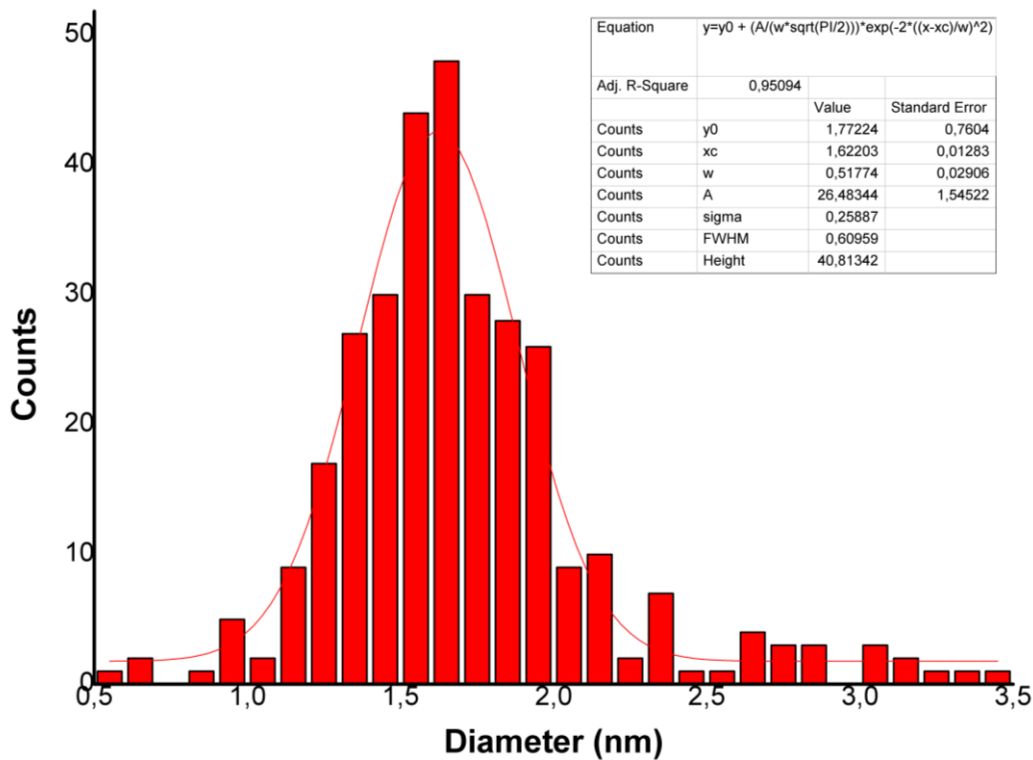


Figure S6: Size distribution of 1-AuNPs. Average diameter $d=1.6$ nm, $\sigma=0.3$ nm.

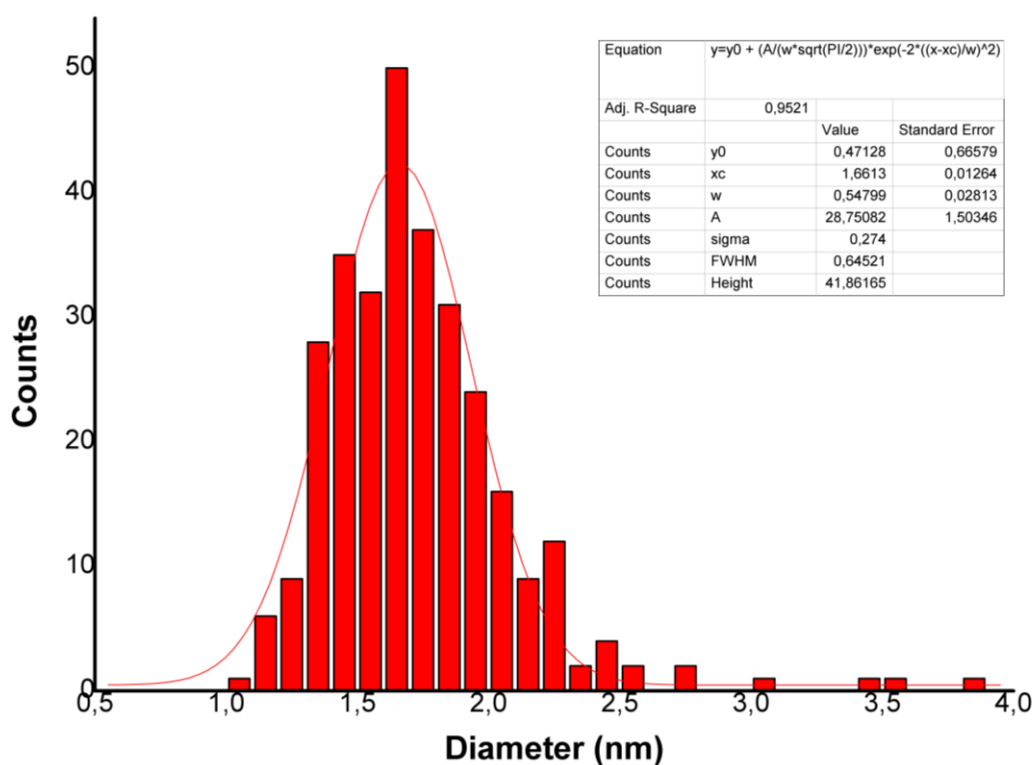


Figure S7: Size distribution of 2-AuNPs. Average diameter $d=1.7$ nm, $\sigma=0.3$ nm.

Combining the data obtained from TEM and TGA analysis (Figures S2-S7) under the same assumptions already described,⁶ the average formula is $\text{Au}_{127}\text{SR}_{50}$ for 1-AuNPs and $\text{Au}_{152}\text{SR}_{80}$ for 2-AuNPs.

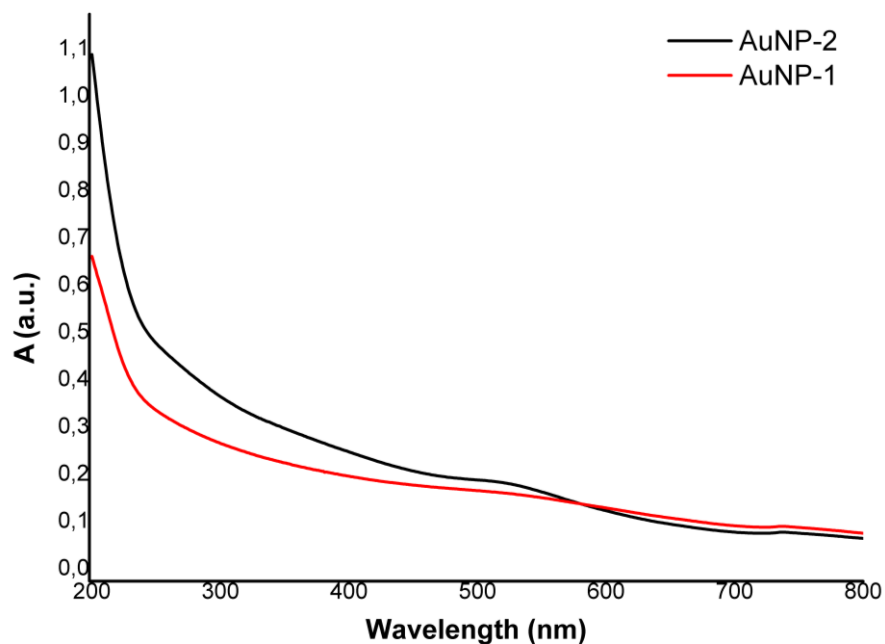


Figure S8: UV-Vis spectra of a solution of AuNPs (0.1 mg/mL). The presence of a weak plasmonic band at 520 nm is due to the presence in the sample of few AuNPs bigger than 3 nm, as visible from the size distribution reported in figures S6 and S7.

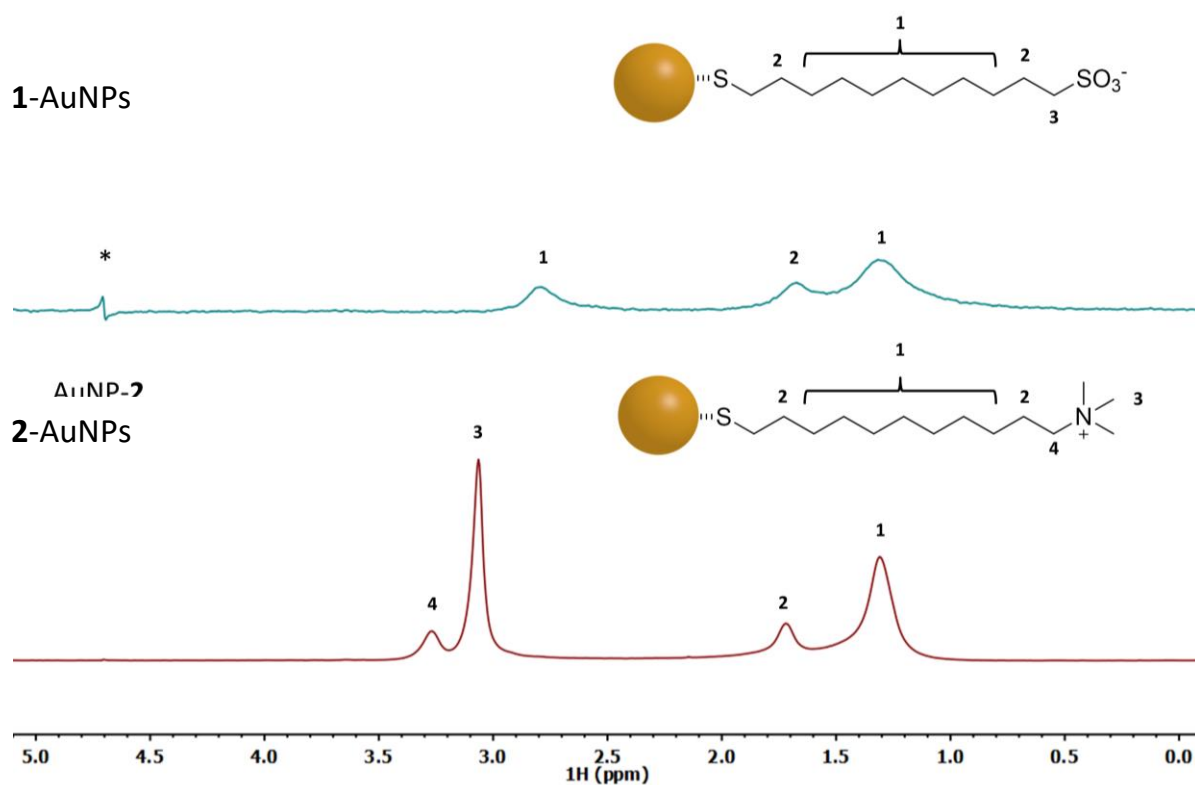


Figure S9: Diffusion filter spectra of a 1 mM solution (expressed as thiol concentration) of 1-AuNPs, top, and 2-AuNPs, bottom. Assignment of the monolayer resonances is reported. In this diffusion experiment only the signals of slow diffusing species are retained. The presence of the thiol signals in this spectrum confirms that it's linked to the AuNPs. The signal of the methylene group next to the thiolate moiety is too broad to be visible in the spectrum. Asterisk denotes the residual water peak.

3. Size of LUDOX[®] nanoparticles

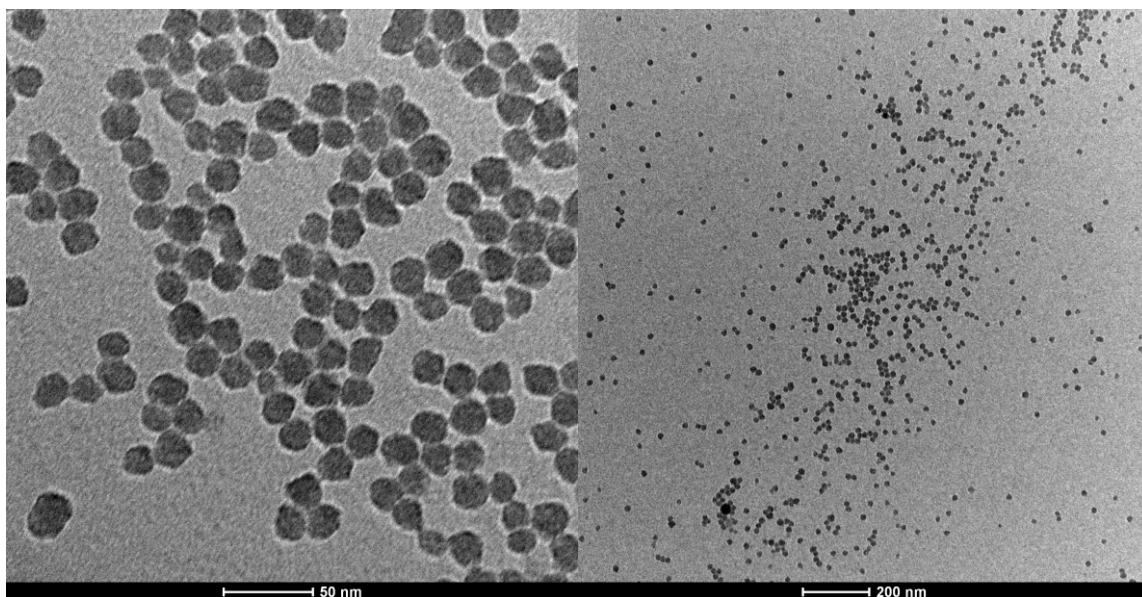


Figure S10: TEM images of a solution of LUDOX[®] HS 30 (0.03% w/w).

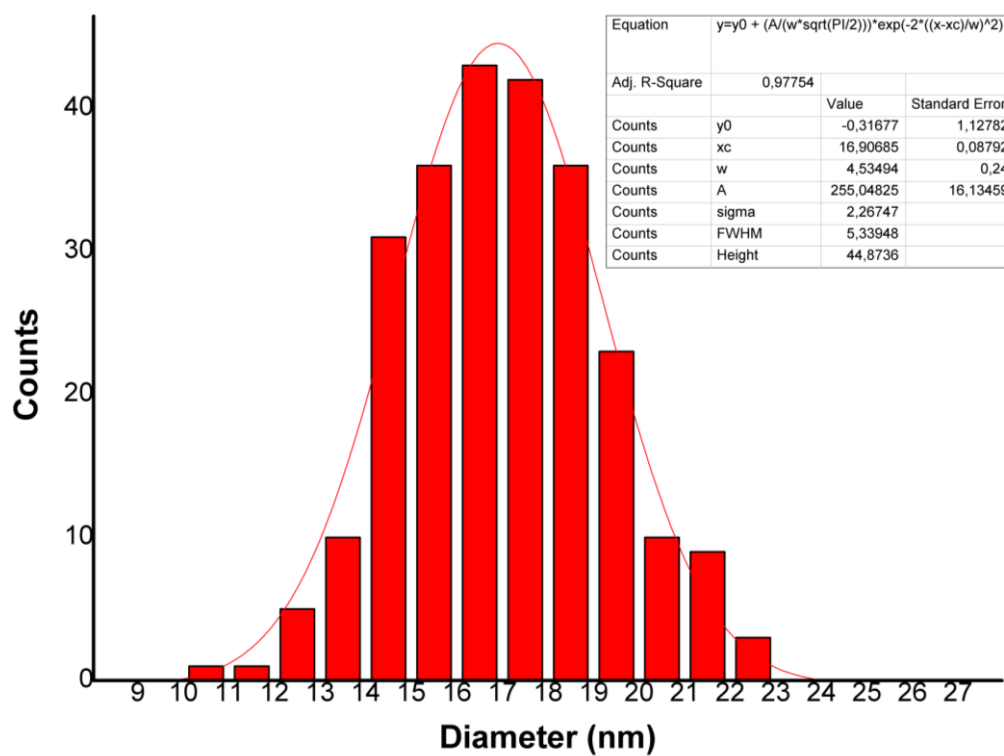


Figure S11: Size distribution of LUDOX[®] HS-30 (16.9 nm σ = 2.3 nm).

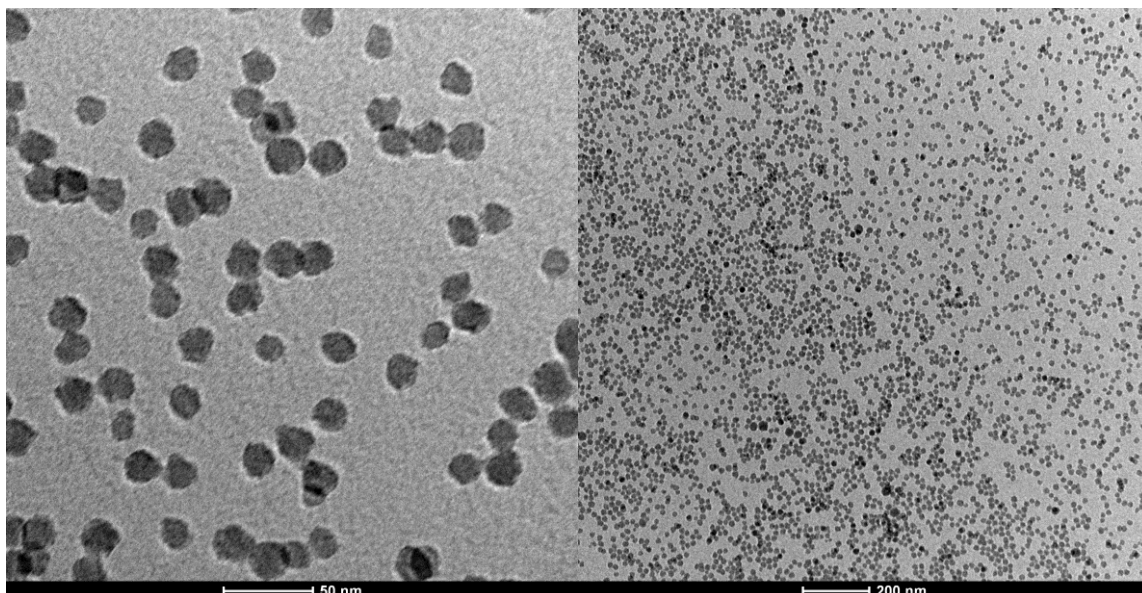


Figure S12: TEM images of a solution of LUDOX® CL (0.03% w/w).

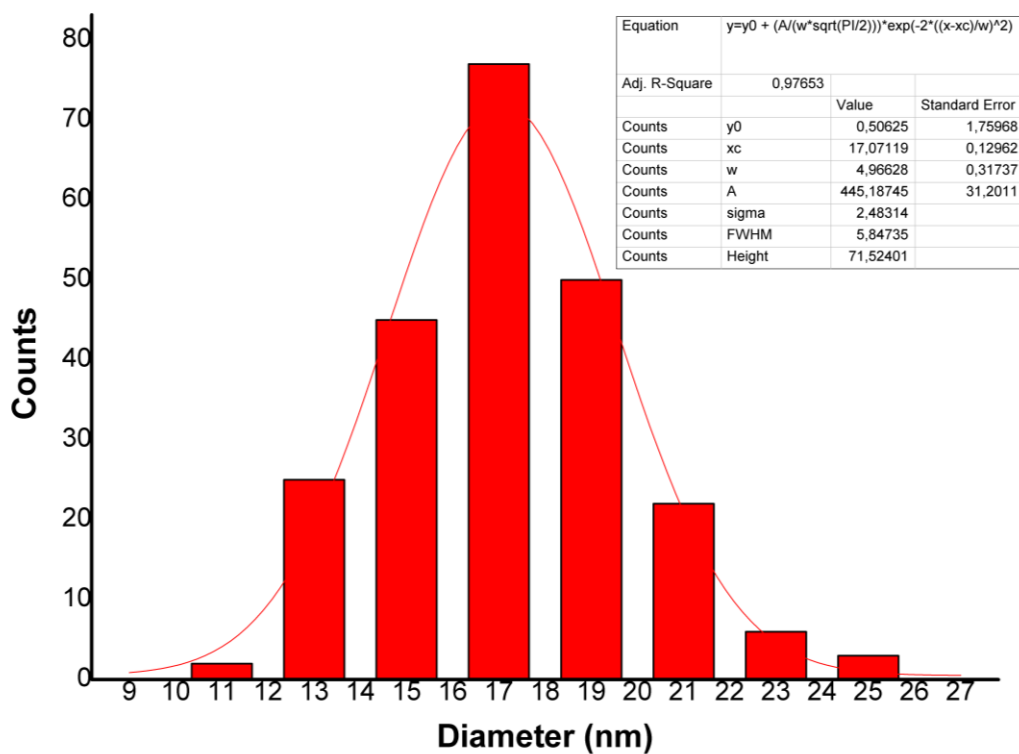


Figure S13: Size distribution of LUDOX® CL (17.1 nm σ = 2.5 nm).

4. DLS experiments

The hydrodynamic particle size and ζ -potential were measured using Dynamic Light Scattering (DLS) with a Malvern Zetasizer Nano-S equipped with a HeNe laser (633 nm) and a Peltier thermostatic system at 25 °C, using a plastic cuvette and a total solution volume of 1 mL. The hydrodynamic particle size of **1**-AuNPs and **2**-AuNPs were measured with an AuNPs concentration of 0.25 mM (expressed as thiol concentration) in phosphate buffer 10 mM. The results reported in the main text are an average of

at least three measures and the error is the standard deviation based on replicate measurements of the mean value. The hydrodynamic particle size and ζ -potential of LUDOX[®] were measured in phosphate buffer 10 mM adding 1 μ L of the commercial 30% w/w suspensions. For completeness, in Figure S14 we report the size distribution histograms by number from a single DLS experiment for both the 1- and 2-AuNPs and HS and CL types of SiO₂NPs as well as the polydispersity index (PDI) and the standard deviations based on the sample distribution statistics.

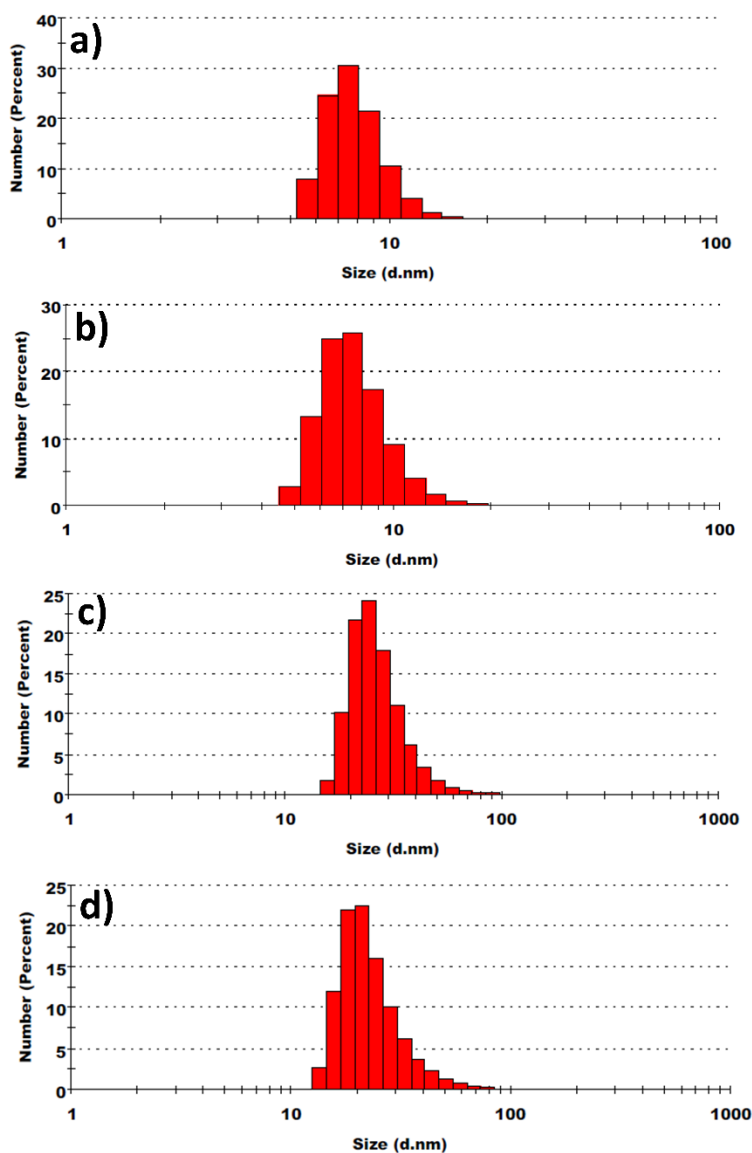


Figure S14: Size distribution histograms by number for a) 1-AuNPs (7.9 ± 1.7 nm PDI: 0.320) b) 2-AuNPs (7.7 ± 2.0 nm PDI: 0.198) c) LUDOX[®]-HS (27.3 ± 8.4 nm PDI: 0.210) d) LUDOX[®]-CL (23.7 ± 9.1 nm PDI: 0.190).

The molar concentrations (in units of nanoparticles) of the commercial 30% w/w LUDOX[®] water suspensions were estimated by assuming a sharp size distribution centred at 17 nm (as determined by TEM analysis) and a homogeneous density of the nanoparticles equal to that of bulk silica (2.65 g/cm^3) for both HS and CL types of SiO₂NPs. Under these assumptions, a single SiO₂NP weighs 6.82×10^{-18} g. 100 g of 30% w/w suspension contains 30 g of silica, hence approximately 44.01×10^{17} nanoparticles (corresponding to $7.31 \mu\text{mol}$ of NPs) that occupy a volume of 11.3 mL. The remaining 70 g of

suspension were assumed to be pure water, resulting in a total volume of the 100 g of colloid equal to 81.3 mL (note that this result is in high agreement with the nominal average density of the commercial colloids of 1.22 g/mL). The molar concentrations (in nanoparticle units) of the 30% w/w suspensions were thus estimated to be about 90 μM for both colloids. This allowed us to calculate the concentration of SiO_2NPs in the suspension under DLS investigation.

DLS measurements in the presence of LUDOX[®] and gold nanoparticles were performed by adding to the SiO_2NPs suspension already under investigation an amount of AuNPs determined *a priori*, assuming that in the nanoconjugates around 60% of the silica surface is coated by the gold nanoparticles. We assumed also that the AuNPs had a radius of 1.8 nm (half the core diameter plus 1 nm to account the length of the thiolate chains). Based on our assumptions we expected around 50 AuNPs to coat each SiO_2NP . Comparing this number with those determined by NMR measurements (section 5 of this manuscript), our DLS measurements have been conducted in a slight excess of AuNPs.

In this last case, an evidence of formation of small aggregates emerged after the analysis of more replicates of the nanoconjugates measures. This is consistent with the evidence of sedimentation noted in absence of PEG and reported in the main text. Size distributions centred in a range from 35 to 80 nm were obtained in samples with the same composition, this for both HS and CL types of SiO_2NPs . As the NMR titrations were reproducible, we believe that this is due to deviations of our system from the ideal DLS system (non-spherical particles, brown solution due to presence of AuNPs...). The presence of small aggregates of 2-4 nanoconjugates is anyways not relevant for the NMR-chemosensing purposes of our system.

The hydrodynamic radii of the AuNPs of about 4 nm, with a solvent shell of 2 nm is in accordance with literature references where hydrodynamic radii of about 4 nm or even larger are often reported for 2 nm gold core nanoparticles in water. In selected cases, DLS measurements were confirmed also by NMR DOSY experiments.^{7,8}

5. Composition of the nanoconjugates

The ¹H-NMR titrations of **1**-AuNPs and **2**-AuNPs with LUDOX[®] CL and LUDOX[®] HS nanoparticles, respectively, allowed us to precisely determine the average composition of the supramolecular nanoconjugates. Based on the calculation in section 4, the 1% w/w water suspensions of LUDOX[®] CL and LUDOX[®] HS SiO_2NPs used in the ¹H-NMR titrations were approximatively 3 μM (in nanoparticles). A total volume of 9 μL of 1% w/w LUDOX[®] CL suspension was added to an NMR tube containing 500 μL of **1**-AuNPs 100 μM in coating thiols (50 thiols per AuNP) before precipitate was observed. In the case of **2**-AuNPs and LUDOX[®] HS NPs, the volume was 7 μL (with now 80 thiols per AuNP). This allowed us to estimate that, on average, each SiO_2NP was coated by a corona of 37 AuNPs for the **1**-AuNPs@LUDOX[®] CL nanoconjugates and 30 AuNPs for the **2**-AuNPs@LUDOX[®] HS nanoconjugates.

6. Samples preparation and NMR pulse sequences

All the NMR spectra in the main text and in the ESI were recorded at 25 °C on a Bruker AVANCE III spectrometer operating at 500.13 MHz ^1H Larmor frequency and equipped with a 5 mm z-gradient broad-band inverse (BBI) non-cryogenic probe. Further details on the NMR experiments can be found in the captions of Figures S15 and S16.

NMR samples were prepared in 1mL Eppendorf vials by diluting the analytes (and eventually the AuNPs) in a mixture of $\text{H}_2\text{O}:\text{D}_2\text{O}=90:10$ in the presence of phosphate buffer and then transferring the resulting solution directly to the NMR tube. Whether present, the right amount of silica nanoparticles (calibrated on the basis of the NMR titrations) was added as the last step. It was done all in one shot with the aid of a micropipette by depositing on the inner wall of the NMR tube one drop of the 1% w/w silica colloid suspended in a 0.01% w/w aqueous solution of PEG2000. After the addition, the tube was vigorously shaken in order to minimize the creation of local concentration gradients of the SiO_2NPs .

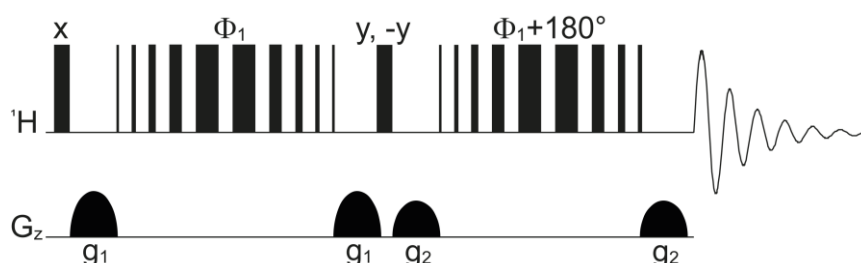


Figure S15: Detection scheme with solvent suppression used to acquire the spectra in panels **a** of Figures 4-6 in the main text. Solvent suppression was obtained through a DPGF-“perfect echo” with W5 clusters as the refocusing element.^{9,10} The delay for binomial water suppression was set to 0.143 ms to avoid sideband effects in the resulting spectra. Pulsed field gradients G_1 and G_2 were set to 22.2 G cm^{-1} and 13.2 G cm^{-1} , respectively. The spectra were acquired with 1024 scans and setting the recovery delay to 2 s.

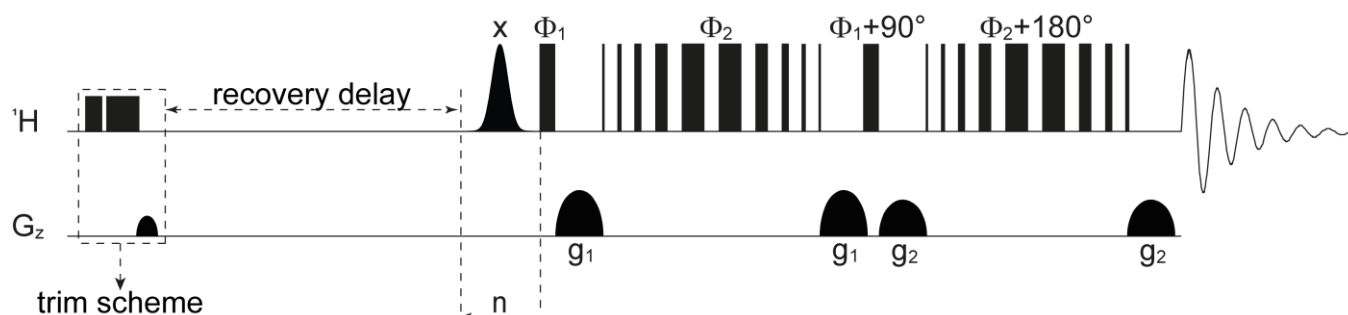


Figure S16: HP wSTD pulse sequence. The solvent suppression scheme is the same presented in Figure S14. The delay for the binomial water suppression was set to 0.143 ms to avoid sideband effects in the resulting spectra. Pulsed field gradients G_1 and G_2 were set to 22.2 G cm^{-1} and 13.2 G cm^{-1} , respectively. The experiments reported in the main text were performed by acquiring 4096 scans and setting the recovery delay to 5.8 s. The high power water saturation was achieved through a train of 40 Gaussian pulses with 1% truncation of length 50 ms each with $\gamma_{\text{H}}B_{1,\text{max}} = 2\pi 750 \text{ rad s}^{-1}$ and setting the RF carrier on resonance with the water signal (2 s of total saturation time).

7. Additional NMR experiments

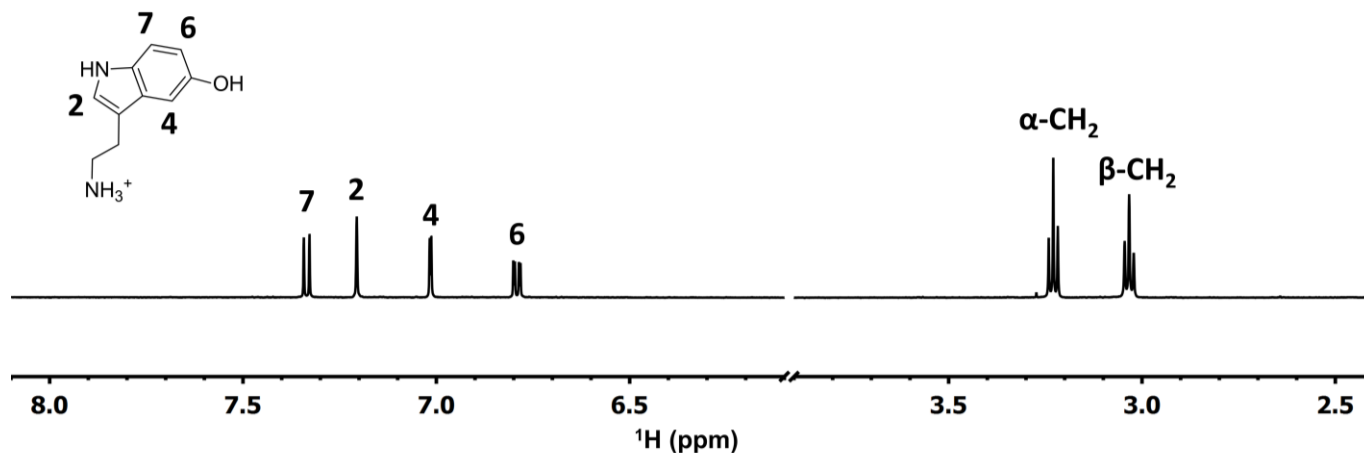


Figure S17: ¹H-NMR spectrum (D₂O, 600 MHz) of serotonin (**3**) 0.5 mM in D₂O δ 7.33 (d, 1H, J= 8.6 Hz), 7.21 (s, 1H), 7.01 (s, 1H), 6.79 (dd, 1H, J= 8.7, 2.3 Hz), 3.23 (t, 2H, J= 7.1 Hz), 3.03 (t, 2H, J=7.0 Hz). Assignations were made according to literature reference.¹¹ The region containing the residual water peak is removed for clarity.

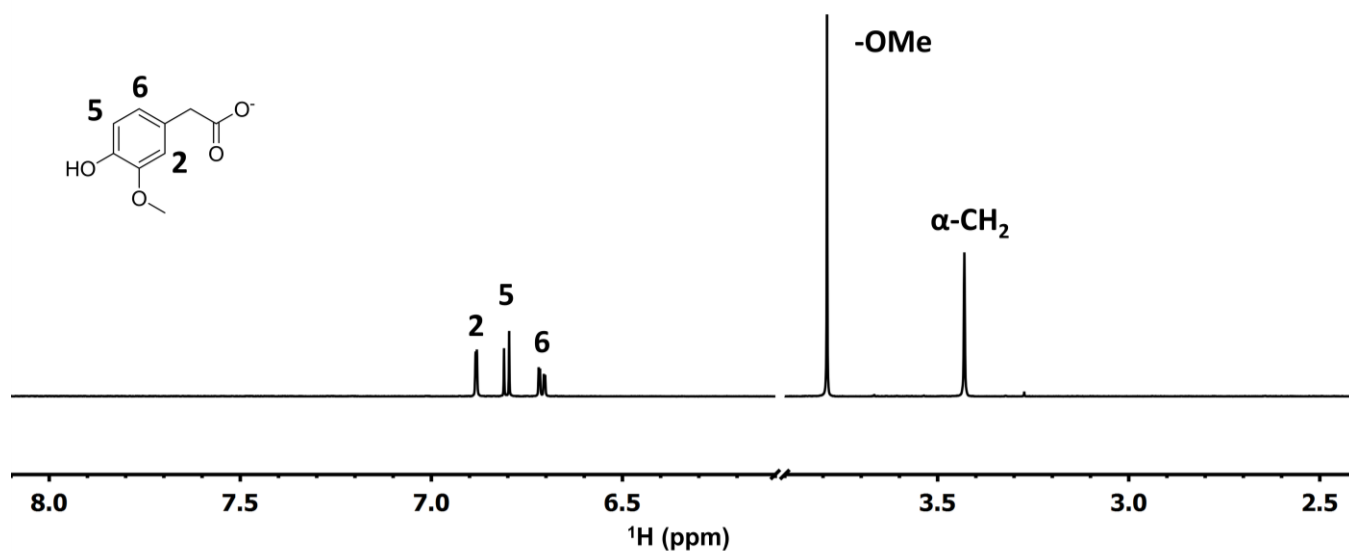


Figure S18: a: ¹H-NMR spectrum (D₂O, 600 MHz) of homovanillic acid (**4**) 0.5 mM δ 6.88 (d, 1H, J= 2 Hz), 6.80 (d, 1H, J = 8.1 Hz), 6.71 (dd, 1H, J = 8.1, 2.1 Hz,), 3.79 (s, 3H), 3.43 (s, 2H). Assignations were made according to literature reference.¹² The region containing the residual water peak is removed for clarity.

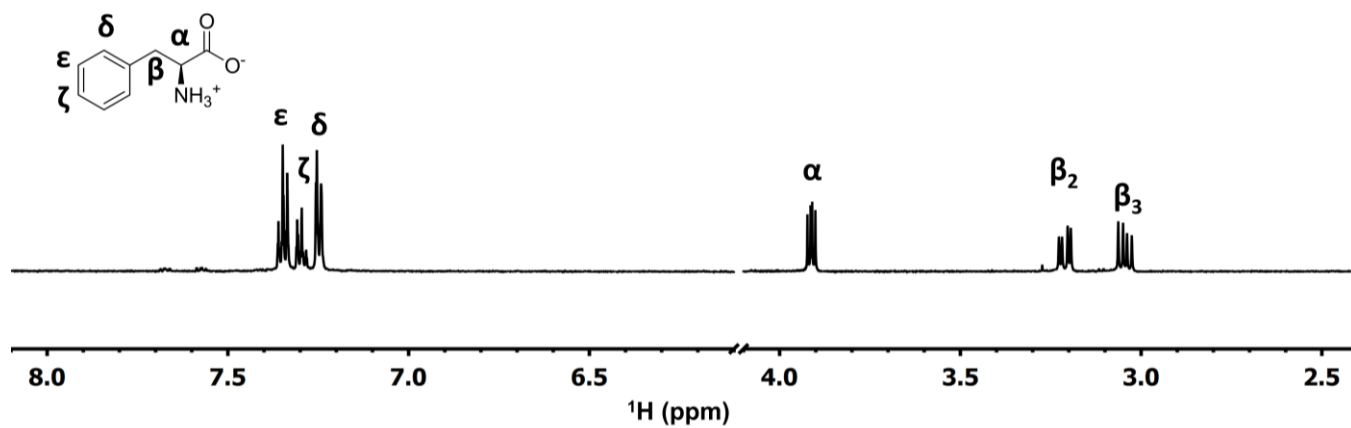


Figure S19: a: ¹H-NMR spectrum (D₂O, 600 MHz) of L-phenylalanine (**5**) 0.5 mM δ 7.34 (m, 2H), 7.30 (m, 1H), 7.25 (m, 2H), 3.91 (dd, 1H, J = 7.98, 5.21 Hz), 3.21 (dd, 1H, J = 14.52, 5.22 Hz), 3.04 (dd, 1H, J = 14.55, 7.95 Hz). Assignations were made according to literature reference.¹³ The region containing the residual water peak is removed for clarity.

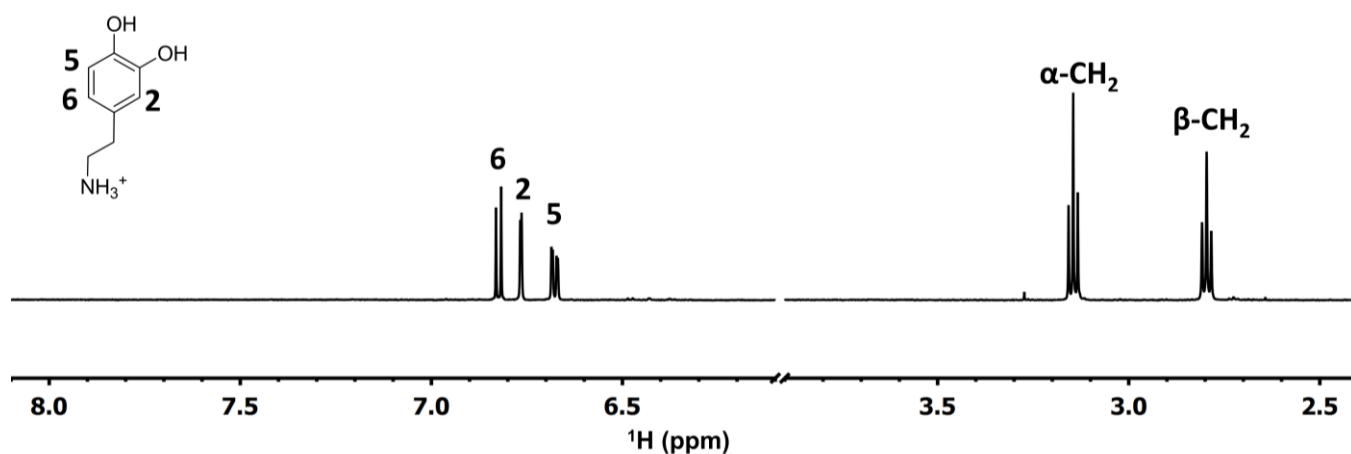


Figure S20: a: ¹H-NMR spectrum (D₂O, 600 MHz) of dopamine (**6**) 0.5 mM δ 6.82 (d, 1H, J = 8.1 Hz), 6.77 (d, 1H, J = 2.1 Hz), 6.68 (dd, 1H, J = 8.1, 2.1 Hz), 3.15 (t, 2H, J = 7.2 Hz), 2.80 (t, 2H, J = 7.2 Hz). Assignations were made according to literature reference.¹¹ The region containing the residual water peak is removed for clarity.

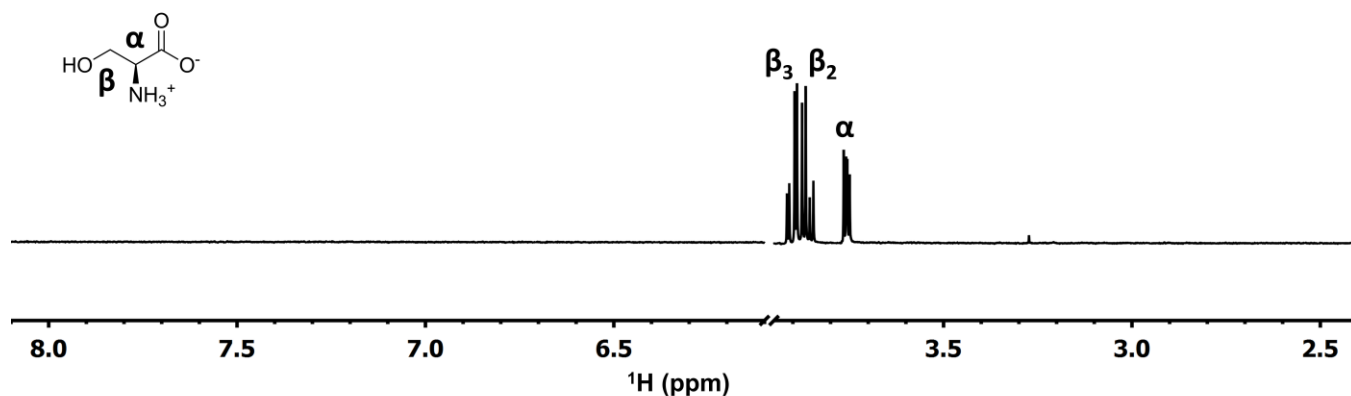


Figure S21: a: ¹H-NMR spectrum (D₂O, 600 MHz) of L-serine (**7**) 0.5 mM δ 3.90 (dd, 1H, J = 12.3, 3.8 Hz), 3.86 (dd, 1H, J = 12.3, 5.8 Hz), 3.76 (dd, 1H, J = 5.8, 3.8 Hz). Assignations were made according to literature reference.¹³ The region containing the residual water peak is removed for clarity.

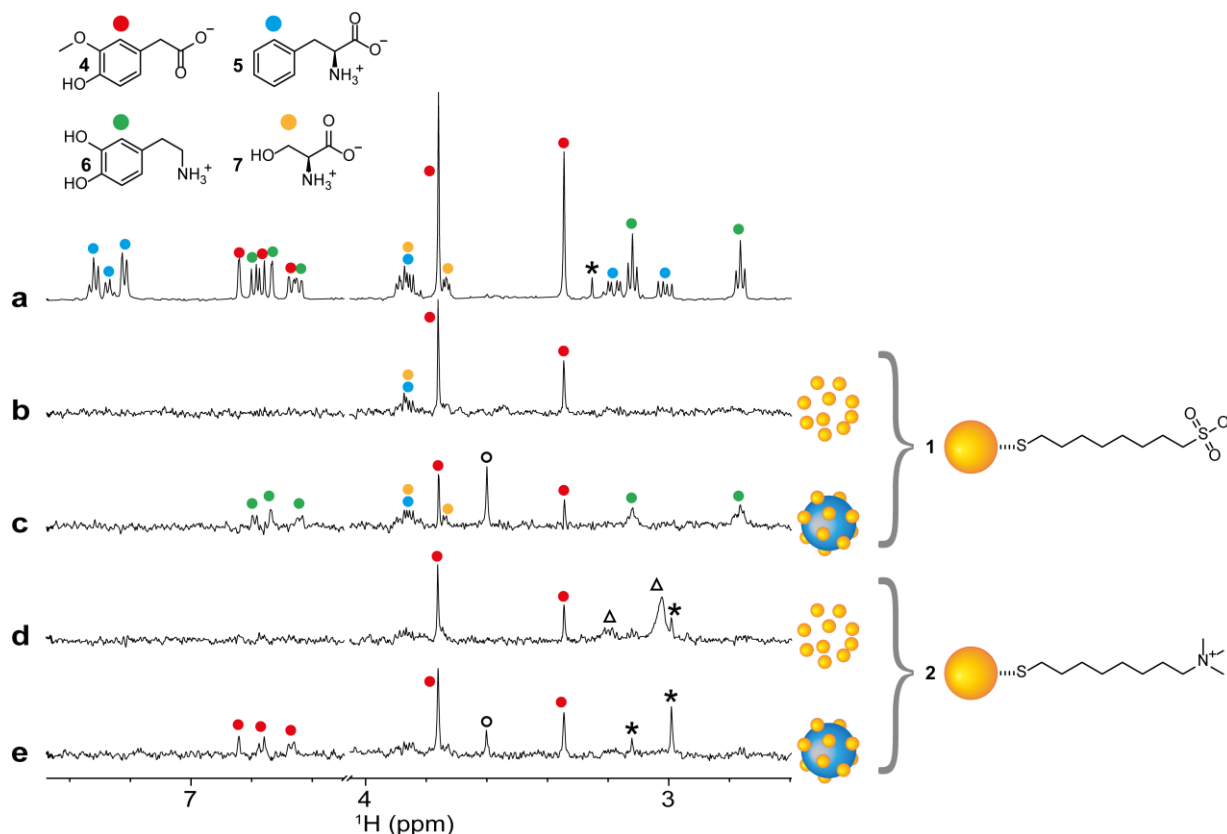


Figure S22: **a:** ^1H -NMR spectrum of a mixture of dopamine (**6**), homovanillic acid (**4**), L-phenylalanine (**5**) and L-serine (**7**) all 20 μM in $\text{H}_2\text{O}:\text{D}_2\text{O}=90:10$ with phosphate buffer (500 μM , $\text{pH}=7$); **b-c:** HP wSTD spectra (4k scans, 4 hours of acquisition time) performed on samples similar to that presented in **a** but in which the concentration of dopamine was lowered to 10 μM . Both HP wSTD experiments were performed in the presence of nanoreceptors (**1**-AuNPs alone in **b** and **1**-AuNPs@LUDOX[®] CL in **c**). In both HP wSTD experiments, the AuNPs concentration was 20 μM in coating thiols. Only in **c** all the resonances of dopamine appear in the processed spectrum. All the other signals in the spectra are false caused by the high RF irradiation power required by the HP wSTD protocol;¹⁴ **d-e:** HP wSTD spectra (4k scans, 4 hours of acquisition time) performed on samples similar to that presented in **a** but in which the concentration of homovanillic acid was lowered to 10 μM . Both HP wSTD experiments were performed in the presence of nanoreceptors (**2**-AuNPs alone in **d** and **2**-AuNPs@LUDOX[®] HS in **e**). In both HP wSTD experiments, the AuNPs concentration was 20 μM in coating thiols. Only in **e** all the resonances of homovanillic acid appear in the processed spectrum. As before, all the other signals in the spectra are false positives caused by the high RF irradiation power required by the HP wSTD protocol. Asterisks and circles denote impurities and the residual PEG2000 signal, respectively. Triangles are used to indicate the residual AuNPs signals.

8. Synthesis of thiols T1 and T2

General: Solvents and all commercially available reagents and substrates were used as received.

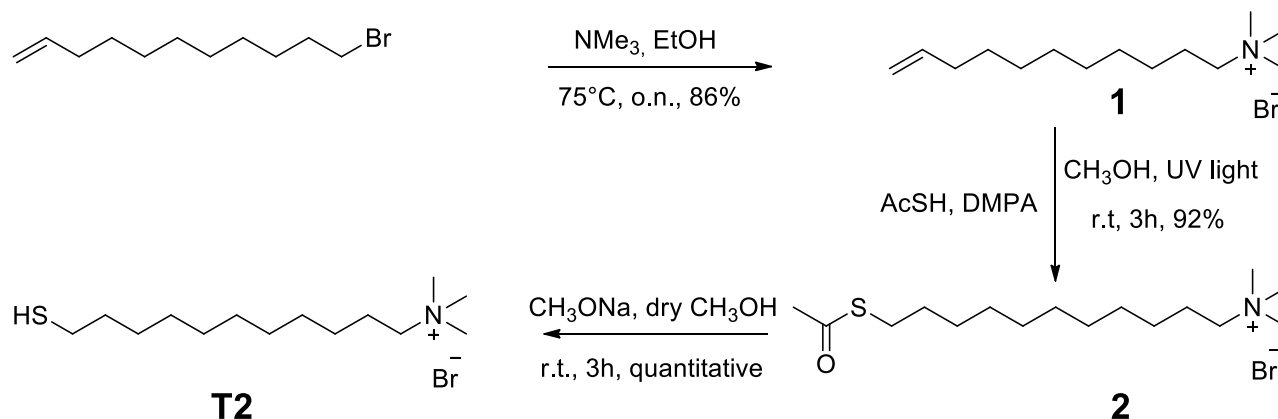
TLC analyses were performed using Merck 60 F₂₅₄ precoated silica gel glass plates. Column chromatography was carried out on Macherey-Nagel silica gel 60 (70-230 mesh).

NMR spectra were recorded using a Bruker AV III 500 spectrometer operating at 500 MHz for ^1H , 125.8 MHz for ^{13}C . Chemical shifts are reported relative to the solvent residual peak. Multiplicity is given as follow: s = singlet, d = doublet, t = triplet, q = quartet, m = multiplet, br = broad peak.

ESI-MS mass spectra were obtained with an Agilent Technologies LC/MSD Trap SL mass spectrometer.

HRMS mass spectra were obtained with a Waters Xevo G2.S (Q-TOF) mass spectrometer (MeOH, 0.5% formic acid).

The thiol **T1** was synthesized following an already reported procedure and the product characterizations matched the ones already reported.⁶



Scheme S1 : Synthesis pathway for the thiol **T2**

N,N,N-trimethylundec-10-en-1-ammonium bromide (**1**)

11-bromoundec-1-ene (1 g, 4.29 mmol, 1 equiv) was dissolved in 10 mL of a 3 M solution of trimethylamine in EtOH (30 mmol, 7 equiv) and kept overnight in a sealed tube at 75°C . The solvent was evaporated through nitrogen bubbling and gentle heating. The residue was triturated in Et_2O and washed three times with cold EtO affording the desired compound **1** (1.23 g, 86%).

$^1\text{H-NMR}$ (MeOD, 500 MHz): δ 1.31-1.46 (br m, 12H), 1.81 (m, 2H), 2.07 (m, 2H), 3.15 (s, 9H), 3.37 (m, 2H), 4.96 (m, 2H), 5.81 (m, 1H).

$^{13}\text{C-NMR}$ (MeOD, 125 MHz): δ 22.53, 25.95, 28.69, 28.74, 28.80, 29.04, 29.07, 33.47, 52.14, 66.46, 133.33, 138.70

ESI-MS: $[\text{M}^+]$ $\text{C}_{14}\text{H}_{30}\text{N}=212.2$

11-(acetylthio)-*N,N,N*-trimethylundecan-1-ammonium bromide (**2**)

1 (500 mg, 1.71 mmol, 1 equiv) was dissolved in 2 mL of MeOH in a quartz cuvette and the solution was degassed under N_2 bubbling for 15 min. Thioacetic acid (367 μL , 5.13 mmol, 3 equiv) and 2,2-dimethoxy-2-phenylacetophenone (DMPA, 43 mg, 0.17 mmol, 0.1 equiv) were added and the mixture was stirred under UV irradiation (365 nm) for 3 h. The solvent was evaporated under vacuum and the residue was triturated in Et_2O and washed five times with cold Et_2O affording the desired compound **2** (580 mg, 92%).

$^1\text{H-NMR}$ (MeOD, 500 MHz): δ 1.30-1.44 (br m, 14H), 1.58 (m, 2H), 1.81 (m, 2H), 2.32 (s, 3H), 2.88 (m, 2H), 3.15 (s, 9H), 3.36 (m, 2H)

$^{13}\text{C-NMR}$ (MeOD, 125 MHz): δ 22.51, 25.93, 28.34, 28.41, 28.74, 28.77, 29.05, 29.08, 29.34, 52.13, 66.49, 196.18

ESI-MS: $[\text{M}^+]$ $\text{C}_{16}\text{H}_{34}\text{NOS}=288.2$

11-mercapto-*N,N,N*-trimethylundecan-1-ammonium bromide (**T2**).

2 (100 mg, 0.27 mmol, 1 equiv) was dissolved in 2 mL of dry MeOH and then sodium methoxide was added (44 mg, 0.81 mmol, 3 equiv). After stirring for 3 hours under N₂ atmosphere, the reaction was quenched adding IR-120 H⁺ resin until pH neutralization, then the resin was filtered off, the solvent was evaporated, giving the deprotected **T2** (86 mg, quantitative), that was directly used for the synthesis of the AuNPs.

¹H-NMR (MeOD, 500 MHz): δ 1.29-1.40 (br m, 14H), 1.56 (m, 2H), 1.74 (m, 2H), 2.87 (m, 2H) 3.08 (s, 9H), 3.29 (m, 2H)

¹³C-NMR (MeOD, 125 MHz): δ 22.66, 25.98, 28.72-29.27, 52.20, 66.46

TOF HRMS: [M⁺] calcd. for C₁₄H₃₂NS=246.2255 Found =246.2279

Spectroscopic data are in agreement with those reported in literature.¹⁵

9. References

- 1 M. Mayer and B. Meyer, *Angew. Chemie Int. Ed.*, 1999, **38**, 1784–1788.
- 2 D. Neuhaus and M. P. Williamson, *The nuclear Overhauser effect in structural and conformational analysis*, Wiley, 2000.
- 3 F. De Biasi, D. Rosa-Gastaldo, X. Sun, F. Mancin and F. Rastrelli, *J. Am. Chem. Soc.*, 2019, **141**, 4870–4877.
- 4 B. Halle, *J. Chem. Phys.*, 2003, **119**, 12372–12385.
- 5 M. H. Levitt, *Spin Dynamics: Basics of Nuclear Magnetic Resonance*, Wiley-VCH, Second Ed., 2008.
- 6 L. Gabrielli, D. Rosa-Gastaldo, M. V. Salvia, S. Springhetti, F. Rastrelli and F. Mancin, *Chem. Sci.*, 2018, **9**, 4777–4784.
- 7 X. Sun, L. Riccardi, F. De Biasi, F. Rastrelli, M. De Vivo and F. Mancin, *Angew. Chemie*, 2019, **131**, 7784–7789.
- 8 L. Riccardi, L. Gabrielli, X. Sun, F. De Biasi, F. Rastrelli, F. Mancin and M. De Vivo, *Chem*, 2017, **3**, 92–109.
- 9 M. L. Liu, X. A. Mao, C. H. Ye, H. Huang, J. K. Nicholson and J. C. Lindon, *J. Magn. Reson.*, 1998, **132**, 125–129.
- 10 J. A. Aguilar and S. J. Kenwright, *Analyst*, 2016, **141**, 236–242.
- 11 G. Gattuso, A. Notti, S. Pappalardo, M. F. Parisi, I. Pisagatti and S. Patanè, *New J. Chem.*, 2014, **38**, 5983–5990.
- 12 K. L. Tuck, P. J. Hayball and I. Stupans, *J. Agric. Food Chem.*, 2002, **50**, 2404–2409.
- 13 M. P. Choules, J. Bisson, W. Gao, D. C. Lankin, J. B. McAlpine, M. Niemitz, B. U. Jaki, S. G. Franzblau and G. F. Pauli, *J. Org. Chem.*, 2019, **84**, 3055–3073.

- 14 B. Cutting, S. V. Shelke, Z. Dragic, B. Wagner, H. Gathje, S. Keim and B. Ernst, *Magn. Reson. Chem.*, 2007, **45**, 720–724.
- 15 P. Thebault, E. Taffin de Givenchy, R. Levy, Y. Vandenberghe, F. Guittard and S. Géribaldi, *Eur. J. Med. Chem.*, 2009, **44**, 717–724.